First-principles study of the optical properties and the dielectric response of Al

Keun-Ho Lee and K. J. Chang
Department of Physics, Korea Advanced Institute of Science and Technology, 373-1 Kusung-dong, Yusung-ku, Daejon, Korea
(Received 28 July 1993)

We investigate the optical properties and the dielectric response of Al through self-consistent *ab initio* pseudopotential calculations. The frequency and wave-vector-dependent dielectric function of Al is calculated for both the real and imaginary parts within the random-phase approximation. The accuracy of the calculations is tested using Kramers-Krönig relations and sum rules. In the limit $\mathbf{q} \rightarrow \mathbf{0}$, we find major optical peaks at 0.5 and 1.5 eV, which originated from the electronic structure, in good agreement with experimental data. For the wave vectors along the [100] direction, the electron-energy-loss function is calculated to examine the plasmon mode. Considering the exchange-correlation and core polarization effects, we find good agreement of the calculated plasma frequencies with experiments. The anisotropy of the plasmon dispersion is also investigated.

I. INTRODUCTION

The problem of the dielectric response function in metals is a long standing one. Knowledge about the dielectric response helps us to understand many important physical properties of interacting electron systems, such as the optical spectrum, the screening of the system to the external longitudinal fields, the electron-phonon interactions, and the lattice dynamics.[1,2] The dielectric function can also describe the collective mode of the density-fluctuation excitation spectrum, i.e., the plasmon mode.

For Al, there have been numerous studies on the electronic structure and the optical properties. At first, the calculations of the dielectric function were mostly performed in the long wavelength limit.[3–5] These calculations showed that the 0.5 and 1.5 eV peaks observed in the absorption spectrum are attributed to the interband transitions between parallel bands in the Brillouin zone. More recently the optical properties of Al in the long wavelength limit were examined by Szmulowicz and Segall using the augmented-plane-wave method[6] and by Maksimov and his co-workers using the linear-muffin-tin-orbital method.[7] Besides, many theoretical and experimental works have been performed on the momentum-dependent plasmon dispersion of Al for testing the exchange-correlation effect. The plasmon dispersion and its anisotropy from the band structure effect were investigated by Bross through the model pseudopotential calculations[8] and by Sturm through the nearly free electron approximation.[9] Although those calculations explained successfully many features of the plasmon dispersion and its anisotropy, their calculated dispersions showed a noticeable deviation from experimental data, especially in the region of large wave vectors.

In this paper we perform first-principles pseudopotential calculations of the dielectric response function of Al. The frequency and wave-vector-dependent dielectric function in the random-phase approximation is calculated for both the real and imaginary parts. In the optical limit $\mathbf{q} \rightarrow \mathbf{0}$, the conductivity exhibits two prominent peaks at 0.5 and 1.5 eV, which arise from the electronic band structure, in good agreement with other theoretical and experimental results. The plasmon mode is examined for the wave vectors $\mathbf{q}$ along the [100] direction by calculating the electron energy-loss function. In the crystal potential, the calculated plasmon dispersion including the exchange-correlation and core polarization effects agrees well with experiments. Comparing the plasmon dispersion along [100] and [111] directions, we also examine the anisotropy of the plasmon dispersion.

The paper is organized as follows. In Sec. II the theoretical background and the calculational details are described. The accuracy of the calculations is also discussed. In Sec. III we present the results and compare with other theoretical and experimental results. Concluding remarks are given in Sec. IV.

II. CALCULATIONS

Using a perturbative technique for independent-particle polarizability, Adler and Wiser formulated the dielectric matrix in the random-phase approximation (RPA):[10,11]

$$\varepsilon_{\mathbf{G}\mathbf{G}'}(\mathbf{q},\omega) = \delta_{\mathbf{G}\mathbf{G}'} - \frac{4\pi}{|\mathbf{q}+\mathbf{G}||\mathbf{q}+\mathbf{G}'|}\frac{2}{\Omega}\sum_{nl\mathbf{k}}\frac{f_l(\mathbf{k}-\mathbf{q})-f_n(\mathbf{k})}{E_{l,\mathbf{k}-\mathbf{q}}-E_{n,\mathbf{k}}+\omega+i\alpha}$$

$$\times \langle l,\mathbf{k}-\mathbf{q} \mid e^{i(\mathbf{q}+\mathbf{G})\cdot\mathbf{r}} \mid n,\mathbf{k}\rangle\langle n,\mathbf{k} \mid e^{-i(\mathbf{q}+\mathbf{G}')\cdot\mathbf{r}} \mid l,\mathbf{k}-\mathbf{q}\rangle \,, \quad (1)$$

where $E_{n,\mathbf{k}}$ and $|n,\mathbf{k}\rangle$ are the energy eigenvalue and the corresponding wave function, respectively, for the nth band at a wave vector $\mathbf{k}$ and $f_{n,\mathbf{k}}$ is the Fermi-Dirac distribution function. We shall use the Hartree unit throughout this work. The local field effects reflected by the off-diagonal elements of the dielectric matrix arise from the inhomogeneous distribution of electron density on the atomic scale and provide a correct description of the dielectric response.[12] The macroscopic dielectric function $\varepsilon_M(\mathbf{q},\omega)$ for $\mathbf{q}$ within the first Brillouin zone (BZ) is related to its microscopic quantities as follows:[13]

$$\begin{aligned}\varepsilon_M(\mathbf{q},\omega) &= 1 \;/\; [\varepsilon^{-1}_{\mathbf{G}\mathbf{G}'}]_{\mathbf{G},\mathbf{G}'=\mathbf{0}} \\ &= \varepsilon_{\mathbf{00}}(\mathbf{q},\omega) \;-\; \sum_{\mathbf{G},\mathbf{G}'\neq\mathbf{0}} \varepsilon_{\mathbf{0G}}(\mathbf{q},\omega)\; M^{-1}_{\mathbf{G}\mathbf{G}'}(\mathbf{q},\omega)\varepsilon_{\mathbf{G}'\mathbf{0}}\;, \end{aligned} \tag{2}$$

where $M^{-1}_{\mathbf{G}\mathbf{G}'}(\mathbf{q},\omega)$ is the inverse of the submatrix $M_{\mathbf{G}\mathbf{G}'}(\mathbf{q},\omega)$ which comprises elements $\varepsilon_{\mathbf{G}\mathbf{G}'}(\mathbf{q},\omega)$ for $\mathbf{G}$ and $\mathbf{G}'\neq\mathbf{0}$. The first term in Eq. (2) contains contributions from band-to-band transitions, while the second term represents the local-field corrections. Neglecting the second term, $\varepsilon_{\mathbf{00}}(\mathbf{q},\omega)$ is just the usual Cohen-Ehrenreich dielectric function, which works well for quasihomogeneous systems such as simple metals.[14] The local fields in covalent semiconductors have an important effect on the macrosopic screening by about 10–20 %. It was also demonstrated that the local field effects induce a shift of optical peaks and a drastic decrease in the magnitude of the optical absorption peak.[15] However, in simple metals, the local field effects are less important[13,16] and neglected in our calculations because of its extensive computational demand.

The macroscopic dielectric function without the local field effects is expressed by the form

$$\varepsilon(\mathbf{q},\omega) = 1 - \frac{4\pi}{q^2}\frac{2}{\Omega}\sum_{n l \mathbf{k}} \frac{[f_l(\mathbf{k}-\mathbf{q}) - f_n(\mathbf{k})]\;|\langle l,\mathbf{k}-\mathbf{q}\mid e^{-i\mathbf{q}\cdot\mathbf{r}}\mid n,\mathbf{k}\rangle|^2}{E_{l,\mathbf{k}-\mathbf{q}} - E_{n,\mathbf{k}} + \omega + i\alpha}\;. \tag{3}$$

As is evident from the formula, only the transitions from occupied states to unoccupied states are considered in the summation. In semiconductors or insulators, since the valence and conduction bands are well separated by the energy gap, only the interband transitions exist. In metals, however, the dielectric function contains contributions from both the intraband and interband transitions. Hence we can rewrite Eq. (3) in the following form:[7]

$$\varepsilon(\mathbf{q},\omega) \;=\; \varepsilon^{\text{intra}}(\mathbf{q},\omega) - \frac{8\pi}{q^2\Omega}\sum_{n\neq l,\mathbf{k}} \frac{[f_l(\mathbf{k}-\mathbf{q}) - f_n(\mathbf{k})]\;|M(n,l,\mathbf{k},\mathbf{q})|^2}{E_{l,\mathbf{k}-\mathbf{q}} - E_{n,\mathbf{k}} + \omega + i\alpha}, \tag{4}$$

where $M(n,l,\mathbf{k},\mathbf{q})$ is the matrix element defined by $\langle n,\mathbf{k}|e^{i\mathbf{q}\cdot\mathbf{k}}|l,\mathbf{k}-\mathbf{q}\rangle$. The first term in Eq. (4) represents the intraband contribution and is expressed as the well-known Drude formula in the limit $\mathbf{q}\to\mathbf{0}$:

$$\varepsilon^{\text{intra}}(\mathbf{q}\to\mathbf{0},\omega) = 1 \;-\; \frac{\tilde{\omega}_p^2}{\omega(\omega+i\gamma)}\;, \tag{5}$$

where γ is the relaxation frequency and $\tilde{\omega}_p^2$ is given by[7]

$$\tilde{\omega}_p^2 \;=\; \frac{8\pi}{3\Omega}\sum_{n,\mathbf{k}} |\nabla E_{n,\mathbf{k}}|^2\;\delta(E_{n,\mathbf{k}} - E_F). \tag{6}$$

The second term in Eq. (4) contains contributions from interband transitions.

The scheme of calculations of the dielectric function is divided into three major parts: the band structure calculations, the evaluations of the matrix elements, and the reciprocal space integration. The band structure of Al is calculated by the *ab initio* pseudopotential method within the local-density approximation (LDA).[17,18] Norm-conserving semi-nonlocal pseudopotentials are generated using the scheme proposed by Hamann, Schlüter, and Chiang.[19] The Wigner interpolation formula for the exchange-correlation potential is used.[20] The valence wave functions are expanded in a plane-wave basis set with a kinetic energy cutoff of 10 Ry.

The linear tetrahedron method is employed to perform the summation over the Brillouin zone.[21] In metals, the k-space summation requires a large number of $\mathbf{k}$-points because of the complexity of the Fermi surface. To describe properly the crossing of energy bands at the Fermi level, a large number of tetrahedrons should be chosen. The tetrahedrons are generated using the scheme proposed by Rath and Freeman.[22] We use 6281 $\mathbf{k}$-points in the irreducible Brillouin zone (IBZ). To check the numerical convergence for the number of $\mathbf{k}$-points, we also use 10 562 $\mathbf{k}$-points in the IBZ. The results from the latter show the negligible difference in the dielectric function, as compared to the former. For the wave vectors $\mathbf{q}$ along the [100] direction, since not the full point symmetry of the fcc structure is associated with $\mathbf{q}$, the integration zone is extended into the one which is six times as large as the IBZ. In this case, approximately 35 000 $\mathbf{k}$-points are required in the extended integration zone. Since the computational demand is considerable if the band structure calculations are performed in the full BZ, we execute the calculations only in the IBZ. The eigenvalues and eigenvectors at the $\mathbf{k}$-points in the other part of the extended integration zone are obtained from those calculated in the IBZ, using symmetry relations. If a $\mathbf{k}$-point in the IBZ is related to another $\mathbf{k}'$-point through one of the symmetry operators, the eigenvalues at the $\mathbf{k}'$-point are identical, and the eigenvectors only differ by phase factors given by a basis rotation with the corresponding

symmetry operator.[23]

In the evaluation of the dielectric function, the number of energy bands is also important. We check the convergence by varying the number of bands. Normally, the calculations of the dielectric matrix require an enormous number of bands, approximately 150–200 bands, for large reciprocal lattice vectors.[12] For our case, however, about 20 bands even for $\mathbf{q} = (\frac{2\pi}{a}, 0, 0)$ are sufficient for obtaining the converged dielectric function.

Finally, the matrix elements in Eq. (4) can be expressed in a simple form when the plane-wave basis set is used. For the wave vector $\mathbf{q} \to \mathbf{0}$, special care must be taken in evaluating the matrix elements due to the nonlocal part of the pseudopotential, which was noted in previous calculations.[12,24] It was shown that the nonlocal pseudopotential contributes about 5–10% to the matrix element in semiconductors. For Al, similar contributions of 5–10% from the nonlocal pseudopotential are found.

III. RESULTS AND DISCUSSION

The calculated energy band structure of Al is shown in Fig. 1 along some symmetry directions. On the symmetry directions, some **k**-points are related to optical peaks in the dielectric function. Overall the calculated band structure agrees well with those of other calculations.[6,8,25] The Fermi energy is estimated to be 11.1 eV from the lowest band at the Γ point in the BZ, while the measured value is 10.6 eV.[26] It was suggested that the overestimation of the valence bandwidth results from the LDA calculation.[16] In Fig. 2, the density of states calculated by the linear tetrahedron method is presented and shows a parabolic feature of bands, especially in the low energy part, with some deviation from the free electron feature in the high energy part. The shapes and positions of several small peaks are quite similar to the results of other calculations.[6,8] We investigate the Fermi surfaces

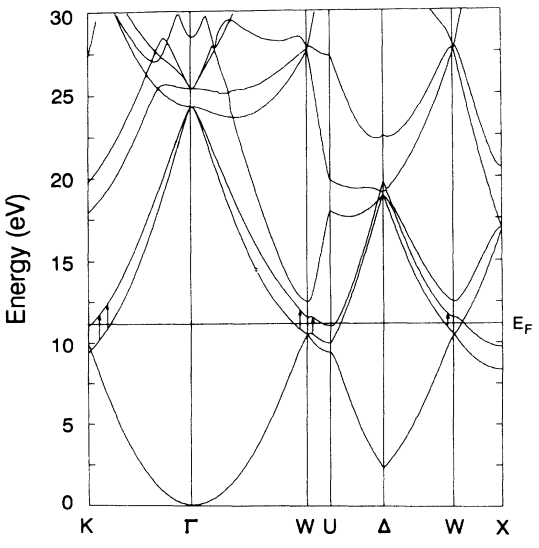

FIG. 1. The band structure of Al is drawn along some important symmetry directions.

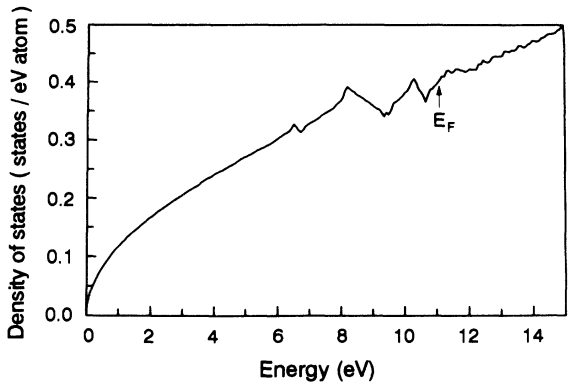

FIG. 2. The density of states calculated by the linear tetrahedron method is shown.

on the Γ-K-W-X plane and find the Fermi surface contours for the second and third zones which are in good agreement with other calculations.[6] However, on the W-X axis, since the crossover point between the second and third bands lies above the Fermi level (see Fig. 1), a small piece of the Fermi surface for the third zone near the W point is not seen.

Figure 3 shows the calculated joint density of states $J(\omega)$. We find two major peaks in $J(\omega)$ at 0.5 and 1.5 eV, which are in good agreement with previous calculations.[6] This result indicates that similar peaks may appear at the same energies in the optical conductivity. We find that these peaks are originated from the electronic band structure. The peak at 0.5 eV results mainly from the transitions between the parallel bands, marked by the arrows in Fig. 1, at the **k** points which lie on the plane made of the W, U, and Δ points in the fcc Brillouin zone. These parallel bands which are degenerate in the free electron case are split by 0.5 eV in the crystal potential. The same analysis shows that the peak at 1.5 eV is attributed to another pair of parallel bands around the Σ-axis on the Γ-K-W-X plane. The electronic origin of the two main peaks is the same as that proposed by Szmulowicz and Segall,[6] however their calculated energy bands were empirically adjusted to yield the parallel band structure. The peak at 1.5 eV is somewhat broader

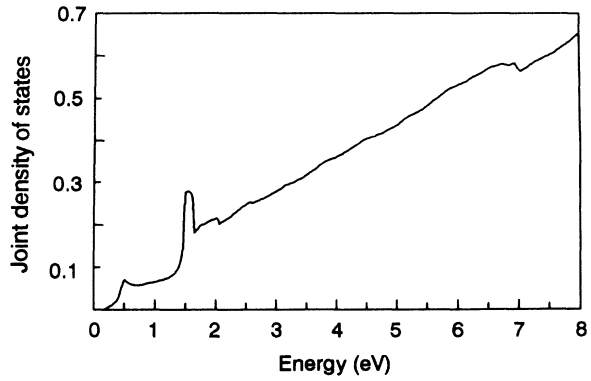

FIG. 3. The joint density of states for Al is drawn in units of states/(eV atom).

than that obtained from the empirically adjusted LDA band.

In the optical limit $\mathbf{q} \rightarrow \mathbf{0}$, as discussed before, the imaginary part of the interband transition term ($\varepsilon_2^{\text{inter}}$) displayed in Fig. 4 shows two peaks at the same energies as those found in the joint density of states. As compared to the 0.5 eV peak, the 1.5 eV peak of $\varepsilon_2^{\text{inter}}$ is rather broad. We find 0.1 eV for the onset frequency of the interband transitions. Brust[4] and Szmulowicz and Segall[6] pointed out that there is no onset frequency as $\omega \rightarrow 0$ due to the accidental degeneracy of the second and third bands on the Γ-K-W-X plane near the Fermi level. Szmulowicz and Segall estimated the value of $\varepsilon_2^{\text{inter}}$ to be about 18 for $\omega = 0$. As mentioned before, however, since the crossover point between the second and third bands on the W-X axis is above the Fermi level in our calculated bands, there is no interband transition in our case as $\omega \rightarrow 0$. The real part of the optical conductivity σ_1^{inter}, which is given in Fig. 4, also shows the onset of the interband transitions at 0.1 eV. Experimentally, Benbow and Lynch[27] showed that σ_1^{inter} becomes negative for ω below 0.25 eV. Although it is not clear yet whether the onset exists or not in the limit of vanishing frequency, overall our calculated σ_1^{inter} agrees well with other theoretical and experimental results. The dielectric function including both the intraband and interband transitions is plotted in Fig. 5. To calculate the intraband contribution to the dielectric function, we have to estimate two parameters, $\tilde{\omega}_p$, which is related to the optical mass, and the relaxation frequency γ. Here we directly calculate $\tilde{\omega}_p$ with the use of the linear tetrahedron method and obtain a value of 12.56 eV which is in good agreement with other estimates in the range of 12.5–13.0 eV.[3,27–29] For γ indicating the contribution of phonons, we use a value of 0.13 eV, which was determined by experiments.[3] As indicated in Eq. (5), the intraband term is found to follow the Drude formula for $\mathbf{q} \rightarrow \mathbf{0}$, which diverges as ω goes to zero. The imaginary part of the Drude dielectric function is usually small, and if the phonon effects are neglected, this term vanishes for finite ω.

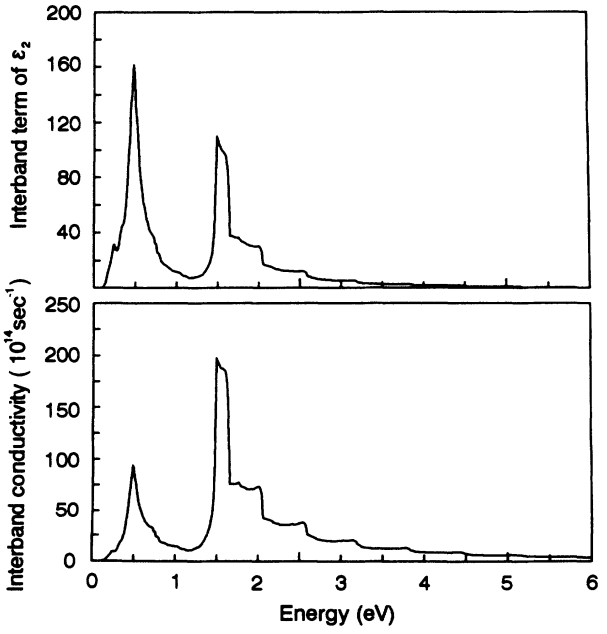

FIG. 4. The imaginary part of the interband term of the dielectric function is plotted in the limit $\mathbf{q} \rightarrow \mathbf{0}$. The interband conductivity is also given in the lower part of the figure.

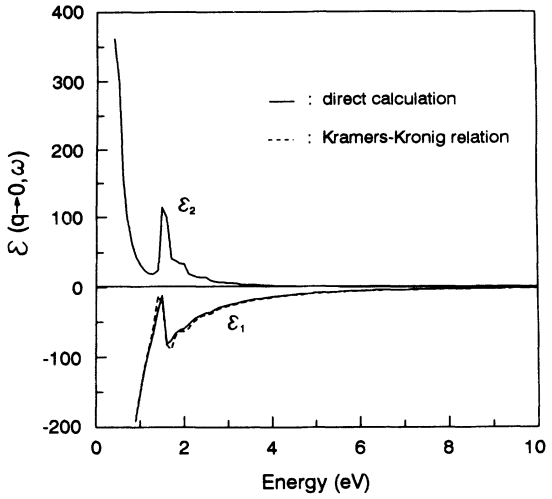

FIG. 5. The real and imaginary parts of the dielectric function in the limit $\mathbf{q} \rightarrow \mathbf{0}$ are plotted by considering both the interband and intraband terms. The dashed lines denote the real part of the dielectric function calculated by the Kramers-Krönig relation.

For the wave vectors $\mathbf{q} = (\frac{1}{4},0,0)\frac{2\pi}{a}$, $(\frac{1}{2},0,0)\frac{2\pi}{a}$, and $(\frac{3}{4},0,0)\frac{2\pi}{a}$, the calculated real and imaginary parts of the dielectric function are presented in Fig. 6. As compared to the $\mathbf{q} \rightarrow \mathbf{0}$ case, we find no diverging behavior in the intraband terms for $\mathbf{q} \neq \mathbf{0}$. As the norm of the wave vector increases, the position of the peak is found to be shifted to the region of higher energies, while the magnitudes of the dielectric function are greatly reduced, indicating that the dielectric function disperses with increasing wave vector. This result is similar to the well-known behavior of the Lindhard dielectric function of a free electron gas. For each $\mathbf{q}$ vector, we test the accuracy of the calculations by evaluating the plasma frequency through the following sum rules:[30]

$$\int_0^\infty d\omega\omega\varepsilon_2(\mathbf{q},\omega) = \frac{\pi}{2}\omega_p^2 , \quad \text{sum rule I,} \tag{7}$$

$$\int_0^\infty d\omega\omega \text{Im}\left[\frac{-1}{\varepsilon(\mathbf{q},\omega)}\right] = \frac{\pi}{2}\omega_p^2 , \quad \text{sum rule II.} \tag{8}$$

As shown in Table I, the calculated plasma frequencies through the sum rules are close to a value of 15.3 eV except for the one calculated from the sum rule I for $\mathbf{q} \rightarrow \mathbf{0}$, while the experimentally measured value is 15.0 eV.[27–29,31–33] We find that the real part of the dielectric function $\varepsilon_1(\mathbf{q},\omega)$ obtained by the Kramers-Krönig relation as for the test of calculational accuracy shows good agreement with the directly calculated $\varepsilon_1(\mathbf{q},\omega)$ for all the wave vectors.

We examine the dispersion of the plasmon mode by calculating the electron energy-loss func-

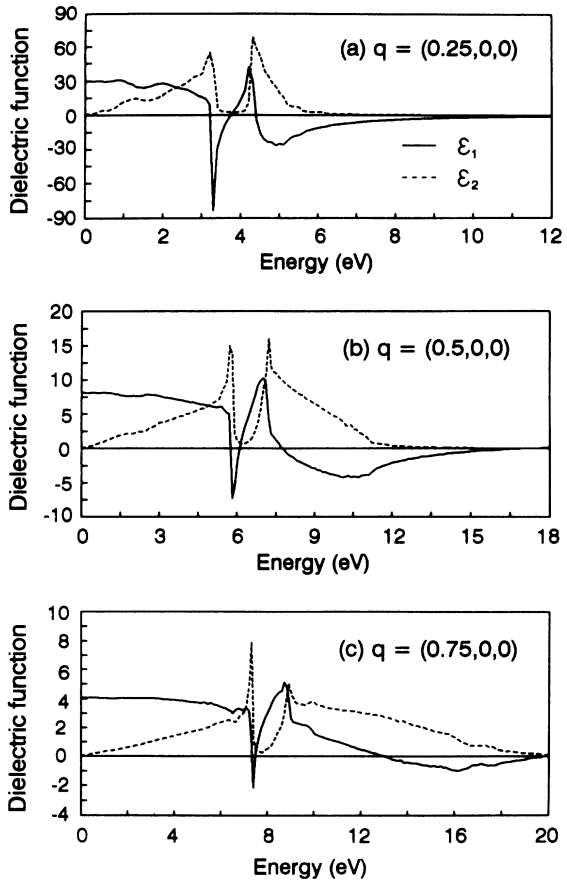

FIG. 6. The real and imaginary parts of the dielectric function are drawn for (a) $\mathbf{q} = (0.25,0,0)\frac{2\pi}{a}$, (b) $(0.5,0,0)\frac{2\pi}{a}$, and (c) $(0.75,0,0)\ \frac{2\pi}{a}$.

tion, $-\mathrm{Im}[\varepsilon^{-1}(\mathbf{q},\omega)]$. The plasmon peak is found to be very sharp at low wave vectors and strongly disperses as the wave vector increases, as illustrated in Fig. 7. This behavior is consistent with the general feature found in simple metals, while broad and nondispersive peaks were found in semiconductors.[13,34] For $\mathbf{q} = (\frac{3}{4},0,0)\frac{2\pi}{a}$, which is in the Landau damping region, a slightly unsymmetrical feature of the plasmon peak with some wiggles is found. In Fig. 8, the calculated plasmon frequencies for the wave vectors along the [100] direction are compared with those of the Lindhard dielectric function and the

TABLE I. The calculated plasma frequencies (in units of eV), $\omega_p(1)$ by the sum rule I and $\omega_p(2)$ by the sum rule II (see the text), are given.

$\mathbf{q}/(\frac{2\pi}{a})$	$\omega_p(1)$	$\omega_p(2)$
(0,0,0)	15.78	15.29
(0.25,0,0)	15.37	15.32
(0.5,0,0)	15.33	15.31
(0.75,0,0)	15.31	15.23

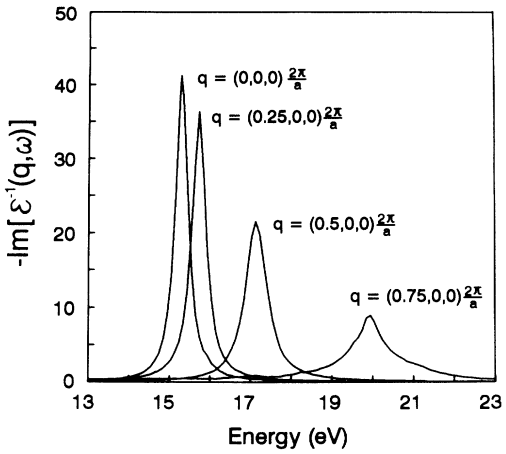

FIG. 7. The imaginary parts of the inverse dielectric function are plotted for several wave vectors along the [100] direction.

experimental results. Since the RPA fails to give a positive pair distribution function at small distances, the exchange-correlation effects are important for large wave vectors. We use the results of Vashishta and Singwi derived for the homogeneous electron gas in the following fashion:[35]

$$\varepsilon(\mathbf{q},\omega) = 1 + \frac{Q(\mathbf{q},\omega)}{1 - G(\mathbf{q})Q(\mathbf{q},\omega)}\ , \tag{9}$$

where $Q(\mathbf{q},\omega)$ is the independent-particle polarizability

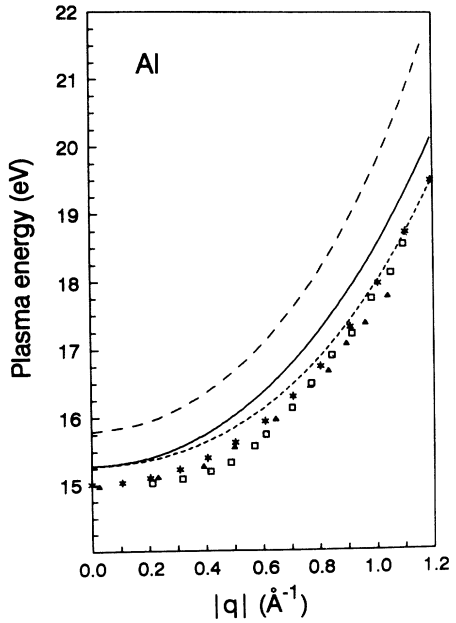

FIG. 8. The calculated plasmon dispersions along the [001] direction are compared with the Lindhard values and the experimental results. The long-dashed line denotes the Lindhard values, the solid line is for the present RPA results, and the short-dashed line is for the results including the exchange-correlation effects. Experimental results are given by boxes (Ref. 31), filled triangles (Ref. 32), and asterisks (Ref. 33).

multiplied by the Coulomb potential and $G(\mathbf{q})$ is the exchange-correlation correction factor. By comparing the present RPA calculations with the Lindhard values, the band structure effect induced by the crystal potential can be estimated. In previous theoretical calculations, Bross and Sturm found weakly wave-vector-dependent downshifts of about 0.3–0.4 eV for the plasma frequencies under the crystal potential.[8,9] However, our calculations show that the downshift due to the band structure effect is more significant and depends on the wave vector. We find the energy shift to be about 0.5 eV for $\mathbf{q} \to \mathbf{0}$ and about 1.2 eV for $|\mathbf{q}| \approx 1.0$ Å^{-1}. As expected, the exchange-correlation correction reduces the plasma frequencies for large wave vectors. Our calculated plasma frequencies with the exchange-correlation corrections are well fitted to a polynomial function, $\omega_p(0) + c_1 q^2 + c_2 q^4$, where the coefficients are 15.28 eV for $\omega_p(0)$, 2.13 eV Å^2 for c_1, and 0.58 eV Å^4 for c_2. With the core polarization effect, we find the further reduction of $\omega_p(0)$ by about 0.35 eV.[36] Thus, the resulting plasmon dispersion is in good agreement with the experimental results within the experimental error.[31–33] Although our results are shown for the [100] direction, the directional average over other lattice directions does not change the dispersion curve significantly. Our results indicate that the description of the plasmon dispersion using two dispersion parameters for c (Refs. 31 and 32) may be improper, consistent with the picture of Sprösser *et al.*, who measured recently the plasmon dispersion of Al.[33] The coefficient c_1 can be regarded as the dimensionless parameter α in atomic units. The Lindhard plasmon dispersion gives a value of 0.44 for α, while our RPA value is estimated to be 0.37. Including the exchange-correlation correction suggested by Vashishta and Singwi in our RPA results, α is estimated to be 0.28, while the experimentally determined value for α is 0.30.[33] Hence, it is clear that both the crystal potential and exchange-correlation effects reduce significantly the Lindhard value for α. We also investigate the anisotropy of the plasmon dispersion between the [100] and [111] directions. At $q = 0.8$ Å^{-1}, we find a maximum anisotropy of about 0.25 eV. It was shown previously that the [110] dispersion curve is slightly above the [111] dispersion in the anisotropic region.[9] In this respect, we expect that the maximum anisotropy between the [110] and [100] directions will be about 0.25–0.30 eV.

IV. CONCLUSION

We have calculated the frequency and wave-vector-dependent dielectric function of Al using the *ab initio* pseudopotential method. In the limit $\mathbf{q} \to \mathbf{0}$, the dielectric function calculated in the random-phase approximation shows two prominent peaks at 0.5 and 1.5 eV, which arise from the interband transitions between the parallel bands. The plasmon mode is examined through the sum rules and the electron energy-loss function. We have found a larger downshift of the plasma frequencies by the crystal potential, as compared to other previous works. The plasmon dispersion with the exchange-correlation and core polarization effects is in good agreement with experiments even for large wave vectors.

ACKNOWLEDGMENTS

This work was supported by the Korea Science and Engineering Foundation, the CTP at Seoul National University, and the Ministry of Science and Technology.

[1] D. Pines, *Elementary Excitations in Solids* (Benjamin, New York, 1963).
[2] W. Hanke, Adv. Phys. **27**, 287 (1978).
[3] H. Ehrenreich, H. R. Philipp, and B. Segall, Phys. Rev. **132**, 1918 (1963).
[4] D. Brust, Phys. Rev. B **2**, 818 (1970).
[5] N. W. Ashcroft and K. Sturm, Phys. Rev. B **3**, 1898 (1971).
[6] F. Szmulowicz and B. Segall, Phys. Rev. B **24**, 892 (1981).
[7] E. G. Maksimov, I. I. Mazin, S. N. Rashkeev, and Y. A. Uspenski, J. Phys. F **18**, 833 (1988).
[8] H. Bross, J. Phys. F **8**, 2631 (1978).
[9] K. Sturm, Z. Phys. B **29**, 27 (1978).
[10] S. L. Adler, Phys. Rev. **126**, 413 (1962).
[11] N. Wiser, Phys. Rev. **129**, 62 (1963).
[12] M. S. Hybertsen and S. G. Louie, Phys. Rev. B **35**, 5585 (1987).
[13] K. Sturm, Adv. Phys. **31**, 1 (1982).
[14] H. Ehrenreich and M. H. Cohen, Phys. Rev. **115**, 786 (1959).
[15] S. G. Louie, J. R. Chelikowsky, and M. L. Cohen, Phys. Rev. Lett. **34**, 155 (1975).
[16] J. E. Northrup, M. S. Hybertsen, and S. G. Louie, Phys. Rev. Lett. **59**, 819 (1987); Phys. Rev. B **39**, 8198 (1989).
[17] J. Ihm, A. Zunger, and M. L. Cohen, J. Phys. C **12**, 4409 (1979).
[18] W. Kohn and L. J. Sham, Phys. Rev. **140**, A1133 (1965).
[19] D. R. Hamann, M. Schlüter, and C. Chiang, Phys. Rev. Lett. **43**, 1494 (1979).
[20] E. Wigner, Trans. Faraday Soc. **34**, 678 (1938).
[21] G. Lehmann and M. Taut, Phys. Status Solidi B **54**, 409 (1972).
[22] J. Rath and A. J. Freeman, Phys. Rev. B **11**, 2109 (1975).
[23] P. J. H. Denteneer and W. van Haeringen, J. Phys. C **18**, 4127 (1985).
[24] S. Baroni and R. Resta, Phys. Rev. B **33**, 7017 (1986).
[25] S. P. Singhal and J. Callaway, Phys. Rev. B **16**, 1744 (1977).
[26] H. J. Levinson, F. Greuter, and E. W. Plummer, Phys. Rev. B **27**, 727 (1983).
[27] R. L. Benbow and D. W. Lynch, Phys. Rev. B **12**, 5615 (1975).
[28] D. Y. Smith and B. Segall, Phys. Rev. B **34**, 5191 (1986).
[29] A. G. Mathewson and H. P. Myers, J. Phys. F **2**, 403 (1972).
[30] G. D. Mahan, *Many-Particle Physics* (Plenum Press, New York, 1981).
[31] K. J. Krane, J. Phys. F **8**, 2133 (1978).
[32] H. Möller and A. Otto, Phys. Rev. Lett. **45**, 2140 (1980).
[33] J. Sprösser, A. vom Felde, and J. Fink, Phys. Rev. B **40**, 5799 (1989).
[34] J. P. Walter and M. L. Cohen, Phys. Rev. B **5**, 3101 (1972).
[35] P. Vashishta and K. S. Singwi, Phys. Rev. B **6**, 875 (1972).
[36] P. C. Gibbons, S. E. Schnatterly, J. J. Ritsko, and J. R. Fields, Phys. Rev. B **13**, 2451 (1976).